Food Chemistry: X 19 (2023) 100793

Contents lists available at ScienceDirect

Food Chemistry: X

journal homepage: www.sciencedirect.com/journal/food-chemistry-x

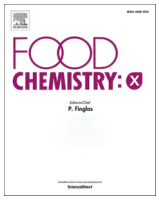

Influence of physicochemical changes and aggregation behavior induced by ultrasound irradiation on the antioxidant effect of highland barley β-glucan

Hongwei Cao [a,b], Xiaoxue Wang [a], Mengmeng Shi [a], Xiao Guan [a,b,*], Chunhong Zhang [d], Yueqin Wang [c], Linnan Qiao [a], Hongdong Song [a,b], Yu Zhang [a,b]

[a] School of Health Science and Engineering, University of Shanghai for Science and Technology, Shanghai, PR China
[b] National Grain Industry (Urban Grain and Oil Security) Technology Innovation Center, University of Shanghai for Science and Technology, Shanghai, PR China
[c] Tibet Himalayan Ecological Technology Co., Ltd., Tibet, PR China
[d] Naval Medical University (Second Military Medical University), Shanghai, PR China

ARTICLE INFO

Keywords:
Highland barley
β-glucan
Ultrasound
Antioxidant
Structure
Aggregation

ABSTRACT

The effect of ultrasonic treatment on the structure, morphology and antioxidant activity of highland barley β-glucan (HBG) was investigated. Ultrasonic treatment for 30 min was demonstrated to improve the aqueous solubility of HBG, leading to a decrease in turbidity. Meanwhile, moderate ultrasound was found to obviously reduce the particle size distribution of HBG, and transform the entangled HBG molecules into flexible and extended chains, which reaggregated to form larger aggregates under long-time ultrasonication. The *in vitro* antioxidant capacity of HBG treated by ultrasonic first increased and then decreased compared to native HBG. Congo red complexation analysis indicated the existence of helix structure in HBG, which was untwisted after ultrasonic treatment. Furthermore, ultrasound treatment influenced the glucopyranose on HBG, which weakened the intramolecular hydrogen bond of HBG. The microscopic morphology showed that the spherical aggregates in native HBG solution were disaggregated and the untangled HBG chains reaggregated with excessive ultrasonication.

1. Introduction

Highland barley has garnered significant attention due to its remarkable health-promoting effects, particularly in terms of its biological activity (Li et al., 2022a). Among its important bioactive constituents, highland barley β-glucan (HBG) stands out as a long-chain polysaccharide comprised of β-D-glucose units linked by β-(1,3) or β-(1,4) glycosidic bonds. HBG exhibits exceptional functionality in emulsification, thickening, water retention, and gelation during food processing. Consequently, current research efforts primarily revolve around optimizing the extraction process and investigating the physicochemical properties of HBG (Al-Ansi et al., 2021). Notably, numerous reports have suggested that HBG holds great potential in regulating blood glucose levels and mitigating constipation (Zang et al., 2023). The biological activities of HBG are closely associated with its antioxidant properties, which enable the termination of oxidative stress reactions through scavenging free radicals (Xi et al., 2023; Xia et al., 2018).

Meanwhile, the free radical scavenging capacity of HBG is heavily influenced by its molecular and structural characteristics. Extensive research findings have indicated that the biological activity of polysaccharides is closely associated with factors such as molecular weight, solubility, viscosity, branching degree, chain conformation, crystallinity and aggregation behavior (Gao et al., 2022; Zhou et al., 2022). However, there remains a dearth of research on the correlation between structural modifications of polysaccharides and their biological activity. Furthermore, processing methods can induce aggregation or structural changes that significantly impact the antioxidant performance of β-glucan. Structural alterations can affect the viscosity and solubility of natural polysaccharides, thereby influencing their biological activity (Ma et al., 2022). Studies have demonstrated that thermal processing-induced reduction in molecular weight leads to a significant increase in the *in vitro* antioxidant activity of β-glucan (Bai et al., 2021). Similarly, the decrease in molecular weight of oat β-glucan enhances immune activity, anti-diabetic properties, anti-proliferation effects, anti-inflammatory activity, and *in vitro* cholic acid adsorption capacity (Błaszczyk et al., 2015). These findings underscore the pivotal role of molecular structure in the biological activity of β-glucan. Nonetheless, whether the biological activity of HBG is influenced by its chemical structures, aggregation

* Corresponding author.
E-mail address: gnxo@163.com (X. Guan).

https://doi.org/10.1016/j.fochx.2023.100793
Received 13 March 2023; Received in revised form 5 July 2023; Accepted 13 July 2023
Available online 18 July 2023

behavior, and other physicochemical changes remains unclear, which hampers the research and development of functional food and health products based on highland barley.

In general, polysaccharides with low molecular weight and low viscosity, devoid of aggregation, are more likely to exhibit enhanced biological activities. However, HBG possesses a relatively large molecular weight and propensity for aggregation, resulting in its diminished antioxidant activity (Cui & Zhu, 2021). Therefore, to explore the potential application of HBG in functional food, it is necessary to improve its antioxidant activity of HBG through appropriate treatment. Ultrasound, as a green processing technology, has found extensive application in polysaccharide extraction and controlled degradation. Ultrasound treatment can reduce particle size, molecular weight, and polysaccharide aggregation, thereby improving solubility and biological activities such as immune regulation, antioxidant, anti-inflammatory, and anti-tumor effects (Yuan et al., 2020). Additionally, ultrasound has a more pronounced impact on polysaccharides with higher molecular weights compared to those with smaller molecular weights, indicating its potential influence on HBG solutions (Wang et al., 2021). The utilization of ultrasound technology offers a simple and eco-friendly approach that promotes the exposure of functional groups, thereby increasing mobility and free radical scavenging activity. Based on this premise, we hypothesize that ultrasound treatment can modify the structure and alter the aggregation behavior of HBG, ultimately enhancing its antioxidant potential. The research results will not only advance the development of the highland barley food processing industry but also provide a scientific foundation for the creation of a range of functional foods and health products with HBG as a key component (Guo et al., 2020; Obadi et al., 2021).

2. Materials and methods

2.1. Materials and chemicals

Highland barley (*Hordeum vulgare* var. *coeleste Linnaeus*) unprocessed grain (blue highland barley, harvest in 2022) was purchased from Tibet Wild Medicinal Materials Co., Ltd (Shigatse, Tibet, China). All highland barley grains were stored in sealed bags below 4 ℃ for refrigeration until use. DPPH (2,2-biphenyl-1-picrylhydrazinyl), ATBS (2,2′- hydrazine bis (3-ethylbenzothiazoline-6-sulfonic acid) diamine salt), thermostable α-Amylase, starch glucosidase and pancreatin were purchased from Sigma-Aldrich (St. Louis, MO, USA). Congo red and dimethyl sulfoxide was provided by Sinopharm Chemical Reagent Co., Ltd. (Shanghai, China). All other chemicals were of analytical grade.

2.2. The extraction of highland barley β-glucan

The extraction of HBG from highland barley grains was conducted according to previous studies with slight modifications (Bai et al., 2021). Raw highland barley was grounded into powder and filtered through a 100-mesh screen. The prepared powder (50 g) was spread in the 150 mm glass culture dish and placed at the center of the microwave Synthesis Platform (XH-200A, Xianghu, Beijing, China) with a 7 W/g power density for 120 s. Briefly, powdered highland barley was suspended in deionized water (1: 20, w/v). The mixture was then centrifuged at 4000 g for 15 min at 80 ℃, the supernatant was combined and concentrated. The HBG extracted from sediment was through enzymatic hydrolysis. Thermostable α-amylase (20,000 U) and starch glucosidase (10,000 U) were used to remove starch, and pancreatin (5000 U) was used to remove protein. The solution was precipitated by 95% ethanol for 12 h, then centrifuged at 4000 g for 20 min to obtain the precipitate. The HBG was freeze-dried and preserved at −18 ℃ for further analysis. Purities of HBG were measured according to the method of AOAC (995.16) using a commercial assay kit (Megazyme International Ireland, Bray, Ireland). The extraction yields of β-glucan were calculated as equation (1):

$$Extractability = \frac{mass\ of\ extracted\ \beta - glucan(g)}{mass\ of\ powered\ highland\ barley\ flour(g)} \quad (1)$$

The basic parameters of HBG were extractability (3.42 ± 0.08 g/100 g flour) and purity (93.42 ± 0.68%).

2.3. Ultrasound treatment of HBG

HBG solution (1%, w/v) was treated by the ultrasonic processor (Model JY92-II DN, Xinyi ultrasonic equipment Co., Ltd, Ningbo, China) under the condition of the ice bath, the ultrasonic temperature was controlled by a circulation system (Chen et al., 2014). The ultrasound treatments were set to a pulse mode (3 s on followed by 5 s off) with a Φ10 mm ultrasonic probe. The ultrasonic probe was dipped 2 cm from the top of the solution. The ultrasonic condition was carried out as previously report with slight modification (Hu et al., 2021). The working frequency of ultrasound is 40 Hz, and the power ultrasound is 900 W. HBG solutions were treated for 0, 10, 20, 30, 40, and 60 min. The samples after ultrasound treatment were labeled as UHBG0, UHBG10, UHBG20, UHBG30, UHBG40, and UHBG60, respectively.

2.4. Determination of solubility and turbidity of HBG

The determination of the solubility of HBG was according to the method of Liu et al. (Liu et al., 2021). The solubility of HBG treated by different ultrasonic conditions was calculated by the following Eq. (2):

$$\text{Solubility} = \frac{m}{M} \times 100\% \quad (2)$$

Where m is the weight of the dried residues from supernatants, and M is the weight of the dry sample.

The determination of the turbidity of HBG was according to Ye et al. (Ye et al., 2021). The absorbance values were recorded at 610 nm using a UV-1800 spectrophotometer (Shimadzu, Japan).

2.5. Determination of antioxidant activity

2.5.1. DPPH radical scavenging activity

The determination of DPPH radical scavenging activity was based on the method of Bai et al. (Bai et al., 2021) with some modifications. HBG solution (1 mL) was mixed with 1 mL of newly prepared dimethyl sulfoxide solution (0.2 mM DPPH) and vortex mixed for 1 min. At the same time, 1 mL of dimethyl sulphite is added to replace the β-glucose solution preparation blank group. The mixture was then kept in the dark at 20 ℃ for 30 min. The absorbance of each reaction solution is measured at 517 nm by a microplate reader (Biotek Epoch 2 T, USA).

2.5.2. Determination of ABTS free radical scavenging activity

The published method (Khan et al., 2016) was used to evaluate ABTS free radical scavenging activity of HBG treated by ultrasonic. The ABTS solution was prepared by mixing 10 mL ABTS (7 mM) with 10 mL $K_2S_2O_8$ (2.45 mM) and reacted in dark at room temperature for 12 h. HBG solution (150 μL of 20 mg/mL) was added to 2850 μL diluted ABTS solution, and the mixture was reacted in the dark for 2 h. The absorbance was then recorded by the Synergy HTX multifunctional microplate reader (BioTek, Biotek Winooski, Vermont, USA) at 734 nm. The HBG in the blank group was replaced with an equivalent amount of Milli-Q water.

2.5.3. Hydroxyl radical scavenging activity

The hydroxyl radical scavenging activity was measured by the method described previously with some modifications (Giese et al., 2015). In brief, 0.5 mL $FeSO_4$ (15 mM) was mixed with 0.35 mL H_2O_2 (6 mM), then 0.15 mL sodium salicylate (20 mM) and 1 mL of HBG (20 mg/mL) were added into the mixture. At the same time, Milli-Q water (1 mL) was used instead of HBG solution was used to prepare a blank group. The

reacted mixture was incubated at 37 ℃ for 1 h, and then the absorbance was measured at 562 nm with a Synergy HTX multifunctional microplate reader (BioTek, Biotek Winooski, Vermont, USA).

2.5.4. Determination of superoxide radical scavenging activity

The superoxide anion radical scavenging activity was determined according to the method described by Bai et al. (Bai et al., 2021) and slightly modified. The reaction mixture (1 mL) consisted of 0.8 mL of HBG, 0.1 mL PMS (0.12 mM) and 0.1 mL NBT (1 mM) was reacted at 25 ℃ for 10 min in the dark. The reaction was terminated by adding 0.04 mL HCl (10 M). The HBG solution was replaced by an equal amount of Milli-Q water. The absorbance at 560 nm was measured with a Synergy HTX multifunctional microplate reader (BioTek, Biotek Winooski, Vermont, USA).

2.6. Measurement of Congo red with HBG

Congo red is dissolved in deionized water and the concentration was adjusted to 2 mM. The HBG solution treated with different ultrasonic treatments was diluted to 1 mg/mL. The NaOH solution was adjusted to the concentration of 0.05, 0.1, 0.15, 0.2, 0.25, 0.3 and 0.4 M (Hu et al., 2021). The resulting samples were supplemented with 1.5 mL of different NaOH solutions, 0.75 mL of treated HBG solution, of 0.5 mL of Congo red solution and 0.25 mL of distilled water. After standing for 20 min, the maximum absorption wavelength (λ_{max}) was measured by a UV-1750 spectrophotometer (Shimadzu Co., Ltd., Japan).

2.7. Particle size distribution of HBG

The particle size of the HBG treated by ultrasound for different time was measured by Zetasizer Nano ZS DLS (Malvern, UK) at 633 nm at a 90° scattering angle of 25 °C (Y. Zhao et al., 2020). The HBG sample was dissolved at 0.1 mg/mL, HBG solution was added to a plastic cuvette and measured.

2.8. Fourier transform infrared spectroscopy (FT-IR)

The FT-IR spectra of native and ultrasound-treated HBGs were recorded on a Nicolet iS50 Fourier Infrared Spectrometer (Thermo Nicolet Inc., Waltham, MA, USA) at room temperature using the KBr-disk method (Luo et al., 2023). Lyophilized powder samples (1 mg) were mixed with 99 mg of KBr was grounded thoroughly and pressed into pellets. The spectra were recorded in the wave number range of 400–4000 cm^{-1}.

2.9. Microstructure of HBG under different ultrasound condition

2.9.1. Transmission electron microscopy (TEM)

The samples were prepared by drop-coating the HBG solution (10 ng/mL) onto the carbon-coated copper grid and then loaded onto a specimen holder (Hu et al., 2021). The morphological characterization of HBG treated by ultrasonic was determined by transmission electron microscopy H-7650 transmission electron microscope (Hitachi, Japan).

2.9.2. Surface morphology of HBG by atomic force microscopy (AFM)

HBG solutions with different ultrasonic time were to 100 μg/mL, followed by drops on the mica plate and air dried in the sterile operation platform (Huang et al., 2022). The mica plate was placed on the operating desk of an AFM (Cypher S, Oxford Instruments Asylum Research Inc., CA, USA), then the images were captured in tapping mode.

2.9.3. Microstructure of HBG by scanning electronic microscopy (SEM)

The microstructure of HBG at different ultrasonic time was determined by Regulus 8100 scanning electron microscope (Hitachi, Japan) at an acceleration voltage of 3 kV, viewed at 65 × and 500 × magnification.

2.10. Statistical analysis

Unless otherwise specified, the experiments were performed in triplicate and repeated at least three times. The experimental data were expressed as mean ± standard deviation (SD). The analysis of variance (ANOVA) was performed, then Duncan multi-range test was conducted. SPSS 26.0 (SPSS Inc., Chicago, IL, USA) was used for statistical analysis, and $P < 0.05$ was considered statistically significant for the results.

3. Results and discussion

3.1. Changes in dissolution properties

The turbidity and solubility reflected the dispersion characteristics of HBG in water. The solubility of HBG increased first and then decreased, reaching the maximum value of 93.6 ± 1.12% at 30 min (Fig. 1A). Ultrasonic treatment improved the solubility of HBG in water within an appropriate time, mainly due to the ultrasonic cavitation effect, which transformed the larger aggregates in HBG into smaller particles. After ultrasonic treatment for a longer time, the HBG solution turned pale white again, which was caused by the reaggregation of small particles (Zhao et al., 2020). Under continuous ultrasound treatment, the heating effect is more pronounced than the cavitation effect, leading to the re aggregation of small particles during excessive ultrasound treatment (Gokce et al., 2014). The turbidity of the HBG solution first decreased and then increased with the extension of ultrasonic time from 0 min to 60 min (Fig. 1B). Without ultrasonic treatment, the turbidity of the HBG solution was relatively high, and reached the lowest turbidity after 30 min of ultrasonic treatment. The turbidity of HBG was related to its solubility, which presented the opposite trends in the solution. It has been reported that ultrasound can affect the turbidity and solubility of HBG (Du et al., 2022). In addition to the molecular weight of a single HBG molecule, the turbidity and solubility also depended on the interaction and aggregation between molecules. The photos of the HBG solution under different ultrasonic time (0–60 min) were shown in Fig. 1C. The HBG solution without ultrasonic treatment was pale white. After a period of ultrasonic treatment (0–30 min), the HBG solution became as transparent as pure water. However, with the further extension of ultrasonic time (>30 min), the HBG solution tended to be turbid and opaque. High-intensity ultrasound will destroy the aggregation behavior of HBG, leading to an increase in solubility. The high-intensity shear force generated by ultrasonic destroyed the force between HBG

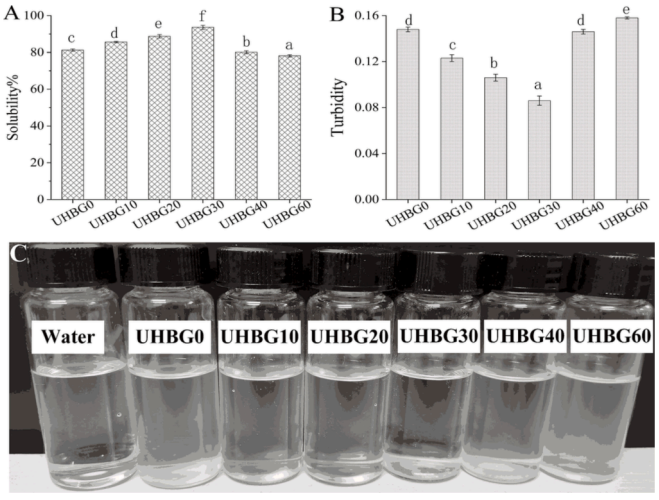

Fig. 1. Solubility (A), turbidity (B) and photographs of HBG solution treated by ultrasound at different time. UHBG0-60 were assigned to HBG solutions ultrasonicated for 0, 10, 20, 30, 40 and 60 min. Error lines indicate the mean ± SDs (n = 3). Different letters (a-f) indicate significant differences ($P < 0.05$).

molecules, which disintegrated the complex structure and exposed the hydrophilic groups of HBG (Du et al., 2022). Ultrasound treatment can significantly improve the solubility of HBG. One reason is that some HBG are degraded by ultrasound, and the molecular weight of HBG decreases, leading to the enhancement of their solubility.

3.2. Particle size distribution of HBG

The conformation of HBG is often characterized by random coil, single helix and multi helix structure, which is affected by intermolecular force, temperature and solvent (Li et al., 2023). Ultrasonic treatment changed the factors that affect the conformation of HBG, therefore, HBG showed different aggregation states. The conformation of HBG refers to the shape and size of HBG in solution, including monosaccharide conformation, flexibility and spatial structure. Particle size distribution is one of the important indicators of the aggregation state of reaction HBG in solution. The volume distribution of HBG treated by ultrasonic at different time (0–60 min) was displayed in Fig. 2. The particle size and polydispersity index (PDI) of the particles were calculated and listed in Table S1. With the extension of ultrasound time, the average particle size of HBG decreased first and then increased. The untreated HBG particle size distribution showed one peak at about 178.25 nm on the volume distribution curve, indicating that there are large particles or aggregates in the HBG solution. This explains why the natural HBG solution appeared pale white. Compared with untreated HBG, the peak positions of UHBG10, UHBG20 and UHBG30 shifted to the left, and the peak position changed from 102.26 nm to 42.36 nm. It showed that ultrasound reduced the particle size, which was due to the change of HBG molecular chain length caused by high-speed shear during ultrasonic treatment. The particle size of HBG is related to the molecular weight, intrinsic viscosity and physical stability. In general, the solubility will increase with the decrease in particle size, while the turbidity will have the opposite trend. The HBG was the solution was damaged obviously after ultrasonic treatment from 0 to 30 min. It can be inferred that the particle size distribution of the HBG is still narrow and uniform when ultrasonic treatment is used to reduce the macromolecular fragments of HBG (Hu et al., 2021). The uniformity of particle size distribution is mainly reflected by PDI, and a smaller PDI indicates a more uniform particle size distribution. In the present study, the PDI values showed a decrease from 0.594 ± 0.035 to 0.382 ± 0.016 with the ultrasonic time increased from 0 to 30 min. However, it is interesting that with the extension of ultrasound time, two peaks appeared in UHBG40 (112.46 ± 6.57 and 447.75 ± 23.65 nm) and UHBG60 (138.64 ± 8.65 and 502.38 ± 32.11 nm) (Table S1). The appearance of large particles indicated the reaggregation of small particles, which promoted the HBG solution turbid and broadened the particle size distribution. The cavitation and shear effects of the ultrasound lead to the reaggregation and entanglement of small particles under the action of excessive ultrasound. In addition, the increased hydrophobic force between HBG molecules after the ultrasonic treatment caused the aggregation of molecules, and some large particles appeared in the solution (Li et al., 2017). When the ultrasonic time is 30 min, the PDI value of HBG is the smallest, indicating that 30 min of ultrasonic is the best ultrasonic time to obtain a smaller and more uniform particle size of HBG. It is worth noting that the HBG/water system without ultrasound showed stable pale white, which may be caused by the formation of micelles by hyperbranched HBG molecules with hydrophobic water as the core and hydrophilic hydroxyl as the shell in the aqueous solution (Wang et al., 2017). These results are consistent with the turbidity and solubility test measurement.

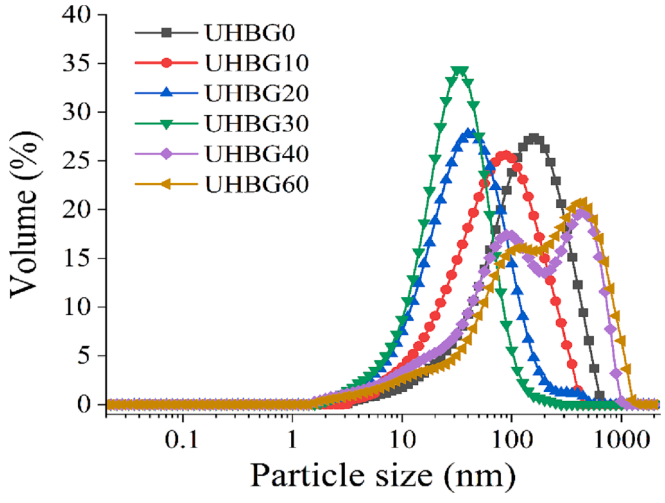

Fig. 2. The particle size distribution of HBG treated by ultrasound at different time. UHBG0-60 were assigned to HBG solutions ultrasonicated for 0, 10, 20, 30, 40 and 60 min.

3.3. Antioxidant property analysis of HBG

Free radicals are associated with many diseases, such as cancer, rheumatoid arthritis, atherosclerosis and AIDS. Antioxidants are very useful for the treatment of these diseases through their scavenging capacity. HBG has the activity of scavenging free radicals, which was greatly affected by its monosaccharide composition, molecular weight, structure and processing methods (Yang & Huang, 2021).

DPPH is a free radical compound, which is widely used to measure the free radical scavenging capacity of various HBG by providing protons and turning yellow in the presence of antioxidants. Compared with HBG without ultrasonic treatment, the percentage of DPPH inhibitory activity of HBG after ultrasonic treatment was shown in Fig. 3A. The enhanced DPPH scavenging activity of HBG was related to the exposure of the active hydroxyl after ultrasonic treatment. Through the DPPH free radical scavenging test of HBG under different ultrasonic time, HBG with the ultrasonic time of 0–30 min has the ability to scavenge DPPH free radicals. Moreover, the DPPH free radical scavenging effect of HBG is greater with the extension of ultrasonic treatment within 30 min. The enhancement of DPPH radical scavenging activity of ultrasonic-treated HBG was due to the low molecular weight subunits during ultrasonic treatment (Alzorqi et al., 2016). However, the DPPH free radical scavenging effect of HBG continued to decline after the ultrasonic time exceeded 30 min, which may be due to the aggregation of HBG. When the ultrasound time exceeded 30 min, the DPPH radical scavenging activity gradually decreased with the extension of ultrasound time. This may be related to the cavitation effect of ultrasound, where the - CH group leaded to the integration of HBG and the formation of clusters in the solution. The presence of clusters reduced the exposure of hydroxyl groups, resulting in a decrease in DPPH scavenging ability (Z. Zhao et al., 2013). Hydroxyl groups can provide electrons to reduce free radicals to a more stable form and/or terminate the free radical chain reaction by directly reacting with free radicals, thereby reducing antioxidant activity of HBG.

Nitrogen-centered stable free radical ABTS is one of the widely used analytical methods to determine the total antioxidant capacity of various extracts. Similar to the advantages of the DPPH method, the ABTS method is also an antioxidant method based on an electron transfer mechanism. The ABTS analysis of ultrasonic-treated HBG is shown in Fig. 3B, which was similar to the determination results of DPPH clearance determination. The ABTS inhibitory activity increased with the ultrasound time from 0 min to 30 min. Compared with the natural HBG without ultrasonic treatment, the inhibitory activity of HBG treated with ultrasonic treatment for 30 min was the highest, which was 84.36%. Tang et al. (Tang et al., 2021) reported that with the increase in degradation of HBG, the reduced molecular weight of HBG improved the ABTS inhibitory activity. HBG with different ultrasonic

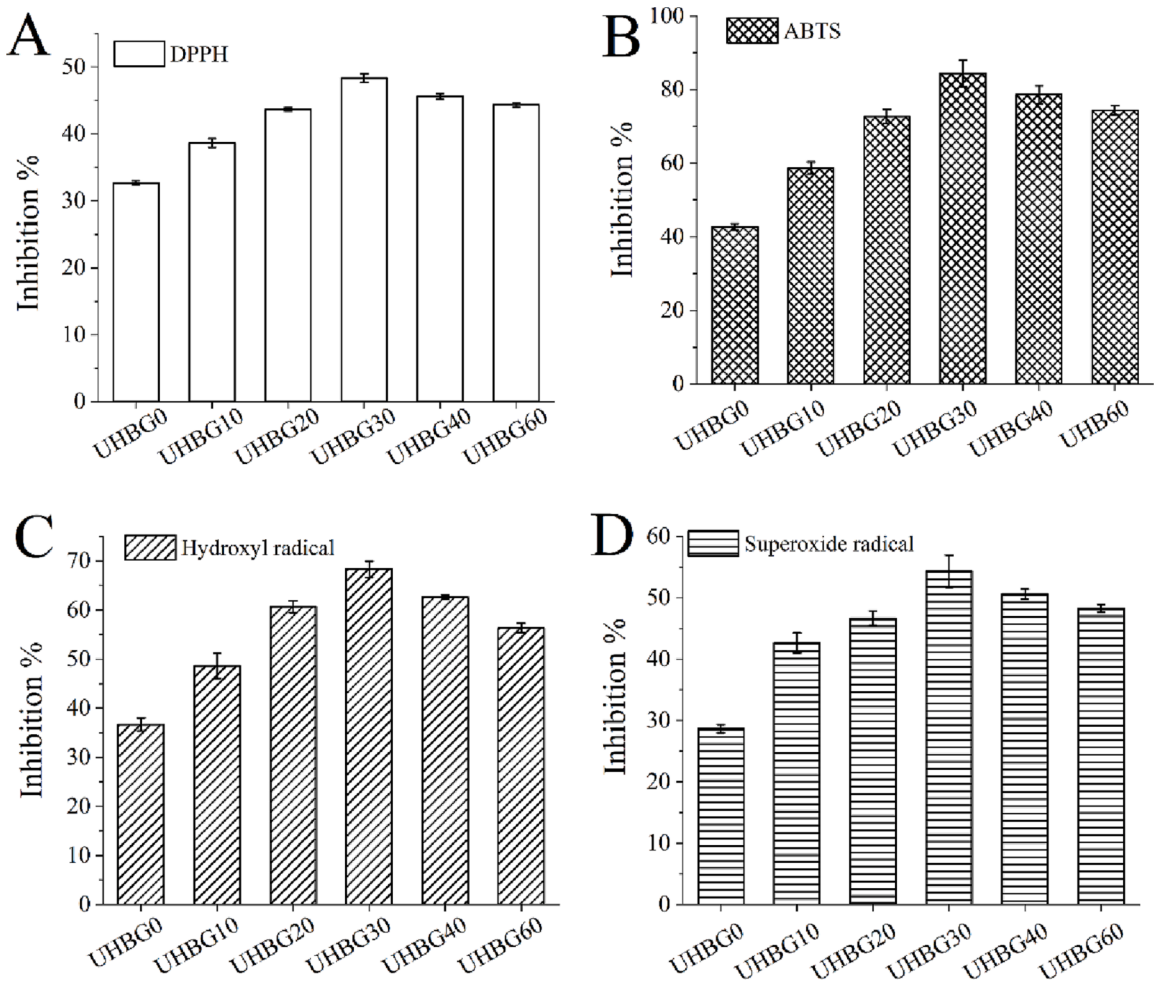

Fig. 3. Scavenging effect of different HBG samples treated by ultrasound for different time on free radicals. A: DPPH radical scavenging activity, B: ABTS radical scavenging activity, C: Hydroxyl radical scavenging activity, D: Superoxide radical scavenging activity. UHBG0-60 were assigned to HBG solutions ultrasonicated for 0, 10, 20, 30, 40 and 60 min.

treatment time (0–30 min) has certain ABTS free radical scavenging activity, which is due to the existence of heteropoly hydrogen atoms that destroyed the free radical chain reaction (Hong et al., 2023). However, the effect of ultrasonic treatment on ABTS radical scavenging was significantly reduced in the range of 40–60 min. In particular, the ABTS scavenging activity of HBG after ultrasonic treatment for 60 min was the lowest after ultrasonic treatment, which was due to the excessive aggregation of HBG loss some groups that can bind to ABTS free radicals. The ABTS radical scavenging activity of HBG displayed same tendency as the DPPH radical scavenging activity after ultrasound treated more than 30 min. Long time ultrasound treatment caused aggregation of HBG, leading to the burial of some active groups, which further decreased the higher scavenging rate of ABTS radicals (Wang, Chen et al., 2021a).

Hydroxyl radicals are very active and can be generated in biological cells through the Fenton reaction. Hydroxyl radicals can cause oxidative damage to carbohydrates, amino acid, protein, nucleic acid and other substances in tissues due to its strong oxidation capacity (Faure & Nyström, 2016). Furthermore, hydroxyl radical has strong biological toxicity in the process of metabolism in animals. Therefore, scavenging hydroxyl radicals is essential to protect organisms or food systems. The hydroxyl radical scavenging capacity of HBG after ultrasonic treatment was shown in Fig. 3C. HBG play an antioxidant role because they can provide hydrogen to free radicals from a stable state to terminate the free radical chain reaction (Chen et al., 2021b). The scavenging capacity of hydroxyl radicals is closely related to the length of ultrasonic treatment. Compared with natural HBG, the percentage of hydroxyl radical scavenging activity in UHBG10 raised by 32.63%. After 30 min of ultrasonic treatment, the scavenging activity of HBG was 68.32%, suggesting that HBG has obvious hydroxyl radical scavenging activity. However, with the further extension of ultrasound time, the inhibitory activity decreased. The results suggested that the hydroxyl group (–OH) of HBG played an important role in antioxidant activity. Hydrogen ions were released from the hydroxyl group of HBG and combined with free radicals that terminate the chain reaction initiated by free radicals (Xiong et al., 2022).

Superoxide radicals are relatively weak oxidants, but they can amplify cell damage by producing other kinds of free radicals and oxidants, such as hydrogen peroxide, hydroxyl radicals and singlet oxygen (Xie et al., 2022). Superoxide anions can also indirectly initiate lipid peroxidation to form H_2O_2, the precursor of hydroxyl radicals was produced. The scavenging effect of ultrasonic treatment of HBG on superoxide free radicals is time-dependent (Fig. 3D). When ultrasonic treatment time is 30 min, the scavenging activity of HBG was 54.32%. However, after ultrasonic treatment for 40 min and 60 min, the scavenging activity of HBG against superoxide free radicals was significantly reduced. Superoxide radicals are reactive oxygen species (ROS) with high activity. HBG can provide hydrogen atoms to eliminate superoxide free radicals, which will be oxidized and degraded, accompanied by glycosidic bond breaking and ring opening (Mosele et al., 2018). The improvement of the antioxidant capacity of HBG was due to the better water solubility of the degraded molecular structure, which enlarged the

contact area between active functional groups and free radicals. The change of spatial structure after ultrasonic treatment weakened the intermolecular force and hydrogen bond force of HBG (Bai et al., 2021). The hydrogen supply capacity was increased, thus enhancing the formation of a more stable structure between hydrogen and free radicals. In conclusion, the detection of various antioxidant indexes under the action of HBG with different ultrasonic time showed that HBG had good antioxidant activity.

3.4. Structural changes of HBG by Congo red complexation

Although HBG molecules cannot form specific α-helix, β-sheet and other secondary structures, some HBG molecules have special spiral structure, which is closely related to the biological activity of HBG (Yan et al., 2021). Therefore, it is necessary to investigate whether HBG has a spiral structure and the effect of ultrasonic treatment on the spiral conformation of HBG. In an alkaline solution, Congo red can form a complex with HBG with single or multiple helix conformation. The maximum absorption wavelength (λ_{max}) of the complex in an alkaline solution at low concentration has a red shift compared to the Congo red, and a metastable region appeared within a certain NaOH concentration range (Zhang et al., 2021). The changes of the maximum absorption wavelengths of the complexes formed by ultrasonic-treated HBG and Congo red in different concentration ranges were shown in Fig. 4. When the concentration of NaOH was <0.2 M, the maximum absorption wavelength of the complex of HBG and Congo red has a significant redshift, indicating the existence of a spiral structure. With the continuous increase of NaOH concentration in the mixed solution (<0.2 M), the maximum absorption wavelength showed a significant downward trend. However, with the further increase of NaOH concentration (>0.2 M), the maximum absorption wavelength (λ_{max}) was almost unaffected. Under strong alkaline conditions, the HBG was gradually degraded. The untwisting spiral structure of the HBG was unable to form the complex with Congo red, which indicated that ultrasound cannot completely destroy the helical structure of HBG, while the high concentration of NaOH can ruin the helical conformation of HBG (Hu et al., 2021). In addition, the comparison before and after ultrasound treatment of HBG showed that HBG under ultrasonic field had a helix structure under weak alkaline conditions. The maximum absorbance of the complex formed by ultrasonic-treated HBG and Congo red at different alkali concentrations is time-dependent. In the low NaOH range (<0.2 M), the maximum absorption wavelength of HBG and Congo red mixed solution decreased and then increased with different ultrasonic treatment time.

The maximum absorption wavelength after ultrasonic treatment was lower than that of natural HBG when the ultrasonic time is 0–30 min, which suggested that ultrasonic treatment caused part of the HBG spiral structure to disintegrate into an irregular coil form. The unfolding of these helical structures led to the decrease in the absorbance. When the ultrasonic time exceeded 30 min, the maximum absorption wavelength (λ_{max}) increased significantly. Ultrasound made the cello-trisaccharide units in HBG easy to form helices through hydrogen bonds and then reaggregated (Wudan Cai et al., 2022). Therefore, it can be inferred that HBG has a helical structure that can be combined with Congo red reagent, and the HBG after ultrasound still remains a certain degree of the helical structure.

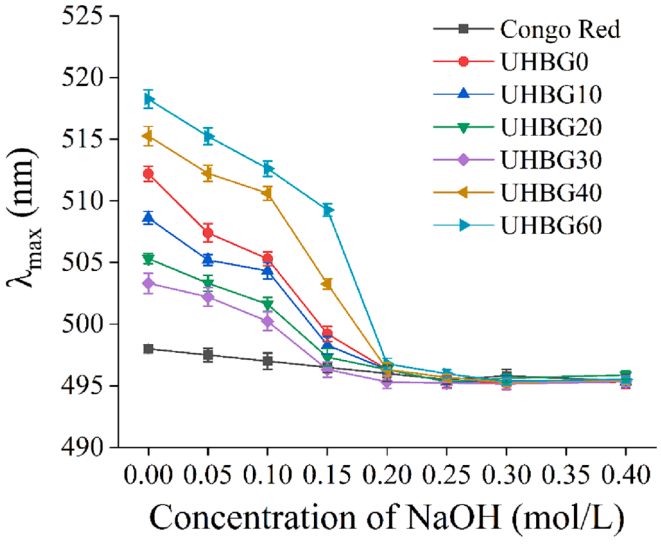

Fig. 4. Changes of maximal absorption (λ_{max}) in the solution of Congo red alone (Congo red), Congo red and HGB ultrasonicated for 0, 10, 20, 30, 40, and 60 min (UHBG0-60) at various NaOH concentrations. (For interpretation of the references to color in this figure legend, the reader is referred to the web version of this article.)

3.5. FT-IR spectroscopy analysis of HBG

FT-IR spectroscopy is an effective tool to analyze the structure of HBG, which can distinguish the characteristic peaks of HBG. The FT-IR spectrum of HBG under ultrasound treated for 0–60 min was shown in Fig. 5. The wide and strong peak at 3275 cm^{-1} is O—H tensile vibration, the weak absorption band at 2890 cm^{-1} represents the saturated hydrogen stretching vibration of C—H in HBG. The peak value of 1643 cm^{-1} is attributed to C—O tensile vibration in the open chain structure of HBG. The absorption peak in 1419 and 1265 cm^{-1} is the variable angle vibration absorption peak of C—H, and the peak at 1156 and 1370 cm^{-1} are attributed to C—O—C tensile vibration and C—O—H bending vibration, respectively (Hu et al., 2021). The above peaks can prove that the sample is a carbohydrate compound. Most notably, the absorption peak between 1200 ~ 800 cm^{-1} is considered as the "fingerprint" area of HBG, including C—O—C, C—C—O and C-OH coupling vibration. In the range of 1200 ~ 1000 cm^{-1}, the overlapping vibration of the side group (C-OH) and glycosidic bond (C—O—C) is helpful for the structural identification of HBG (Y.-C. Li et al., 2022b). The infrared spectrogram of HBG has a relatively strong peak at 1018 cm^{-1} combined with a shoulder peak at 995 cm^{-1}, which is a typical characteristic peak of HBG. In addition, a monosaccharide with pyran ring configuration is also found in HBG. The characteristic peak of the "fingerprint area" of the HBG (895 cm^{-1}) is linked by the type I glycoside bond. In addition, the characteristic peak of the "fingerprint area" of HBG (895 cm^{-1}) linked by the β-type glycosidic bond of monosaccharide with pyran ring configuration was also found in HBG (Li et al., 2021). The absorption peak at 895 cm^{-1} is the characteristic absorption peak of C—H in the β-type glycoside bond, which indicated that HBG has β-structural characteristics. Furthermore, the absorption peaks at 1070 and 1156 cm^{-1}

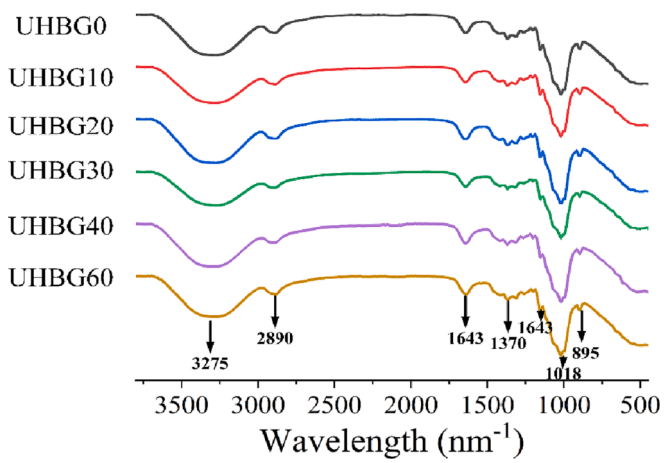

Fig. 5. Fourier transform infrared (FTIR) spectrum of HBG ultrasonicated for 0, 10, 20, 30, 40, and 60 min (UHBG0-60).

belong to C—O—C stretching, which proved that the linear structure of HBG is connected by β-1–3 linkage (Bai et al., 2021).

Compared with untreated HBG, the absorption peaks of ultrasonic-treated HBG at 3275, 2890, 1643, 1370, 1156 and 895 cm^{-1} had no significant change. All these characteristic peaks will appear in the FT-IR spectrum as long as there are sugar units in the ultrasonic-treated HBG, which indicated that the ultrasonic-treated HBG groups are basically the same. The results further revealed that the primary structure of HBG was retained, which means that ultrasonic treatment did not cause serious damage to the skeleton structure of HBG. In addition, we normalized the FT-IR spectra to compare band intensity. Interestingly, the peak intensity at 3275 cm^{-1} of HBG became stronger after ultrasonic treatment, which confirmed that the degradation of larger molecular weight may expose more hydroxyl groups (Liu et al., 2021). These hydroxyl groups mean that there are more opportunities to form hydrogen bonds in HBG. Wang et al. (2021) reported a similar phenomenon. They found that the relatively extensive absorption at 3275 cm^{-1} was due to the O—H vibration generated by the interaction between/within hydrogen bonds in

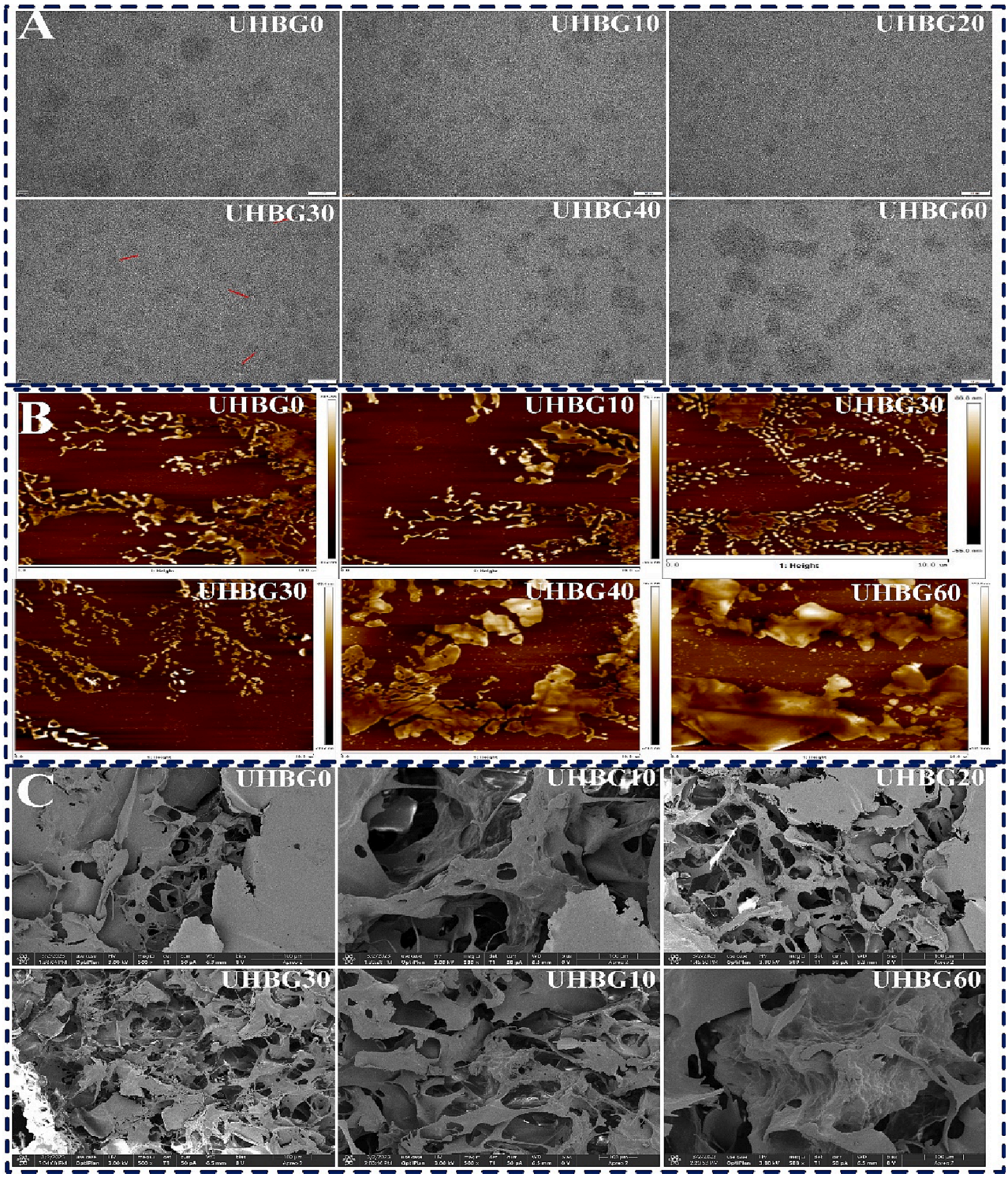

Fig. 6. Microstructure morphology of HBG ultrasonicated for 0, 10, 20, 30, 40, and 60 min (UHBG0-60). TEM (A), AFM (B), AFM (C).

the HBG. However, after ultrasonic treatment for more than 30 min, the peak intensity at 3275 cm^{-1} of HBG became significantly weaker after ultrasonic treatment, which may be due to the O—H vibration being covered up by the aggregation of HBG molecules caused by ultrasonic treatment. The results were consistent with the results of antioxidation.

3.6. Microstructure and morphological observation

Ultrasonic treatment influenced the aggregation behavior of HBG, the microscopic morphology of HBG after ultrasonic treatment by TEM was shown in Fig. 6A. Natural HBG mainly existed in the form of large spherical aggregates, and no chain molecules form was observed. The polymer particles were formed between molecules in the form of intertwining, many HBG molecules were entangled and cross-linked to form large spherical aggregates (Xu et al., 2022). After ultrasonic treatment, the spherical aggregates of HBG gradually depolymerized, and some sample particles with significantly reduced size appeared. In the process of ultrasonic treatment of HBG, macromolecular entanglement is reduced due to the change of HBG chain structure, and then the morphology of HBG was greatly changed. These morphological changes were attributed to the decomposition of HBG by ultrasonic energy (Hu et al., 2021). In addition, some transparent bubbles (red arrow) can be seen in Fig. 6A (UHBG30), which may be cavitation bubbles that did not collapse during the ultrasonic process. It means that large HBG aggregates were disintegrated due to cavitation effects. Ultrasound stretched the structure of HBG (UHGB30), resulting in a uniform distribution in water. However, the groups exposed from HBG precipitated the reaggregation of previously separated HBG chains through intermolecular interaction, resulting in an increase in turbidity and particle size of UHBG40 and UHBG60 (Cai et al., 2018). AFM was further used to evaluate the structural changes and morphology of HBG after ultrasound treatment (Fig. 6B). The natural HBG aggregates presented the shape like a “mountain range” with some small molecules that are not aggregated (Hu et al., 2021). Due to the existence of a large number of hydroxyl groups in HBG, the intramolecular forces promote the crosslinking between HBG molecular chains (Feng et al., 2021). In addition, large numbers of hydrogen bonds interact with water molecules in HBG molecules, which makes the space structure of HBG adsorb more water molecules. Therefore, it is easier for HBG to polymerize the multistrand chains together, which is also the reason why HBG has high viscosity. After ultrasonic treatment for 10 min, in addition to large aggregates, filament-like structures also appeared (Zheng et al., 2021). According to the FT-IR analysis results, this may be due to the influence of ultrasonic treatment on HBG glucopyranose, which weakened the intramolecular hydrogen bond of HBG. Compared with natural HBG, UHBG10 showed great changes in morphology, that is, aggregates formed by crosslinking were attacked by ultrasonic cavitation, resulting in its dispersion into smaller particle aggregates. With the prolongation of ultrasound time (10–20 min), the aggregation behavior of HBG was significantly reduced, and the aggregation chain and strip adhesion structure changed into the stretch chain state. After 30 min of ultrasound, the number of aggregates continued to decrease, resulting in a decrease in particle size. HBG molecules were easier to combine with water molecules to improve the stability of HBG (Chen et al., 2021b). However, with the further extension of ultrasound time, large aggregates appeared in UHBG40 and UHBG60. The morphology of the aggregates has also changed significantly, showing a soft and fluffy sponge shape. The interaction of hydrogen bonds between or within the molecular chains caused the association of HBG to form aggregates of different shapes, which is consistent with the solubility and particle size results reported previously (Hu et al., 2021). Based on SEM images (Fig. 6C), it can be inferred that ultrasound can greatly affect the structure of HBG in a time-dependent pattern. Specifically, HBG without ultrasonic treatment is mainly characterized by spherical aggregates with chain winding. UHBG10 and UHBG20 destroyed the spherical aggregate structure formed by intertwining, but a small amount of HBG formed irregular spherical particles with smaller sizes. After ultrasonic treatment for 30 min, most HBG macromolecules were stretched under the effect of ultrasonic cavitation, which led to the full contact between the external hydrophilic hydroxyl groups of HBG and water. The distribution of HBG molecules became more uniform, indicating that ultrasound further promoted HBG evenly distributed in the liquid (Chen et al., 2014). After 30 min of ultrasonic treatment, the HBG solution became clear and transparent, showing strong antioxidant activity. The HBG in UHBG40 and UHBG60 was further separated, which made it difficult to form the hydrophobic association and reassemble the chains to form larger aggregates. A long time of ultrasonic treatment (40–60 min) will cause the separated and stretched chains to reassemble, leading to an increase in the turbidity of HBG. As a result, the turbidity of HBG increased. With the decreasing of the solubility, the solution of HBG became pale white again, thus reducing the antioxidant activity. Therefore, the structure of HBG can be well controlled by adjusting the ultrasound time to change its antioxidant activity. In order to obtain an HBG solution with high antioxidant activity, it is recommended that the ultrasonic time should not exceed 30 min.

4. Conclusion

The present work evaluated the effects of different ultrasonic time on the structure, and morphology of HBG. Ultrasonic treatment within 30 min improved the water solubility of HBG, changing its color from pale white to transparent. Meanwhile, the solution became turbid with the increase of particle size after ultrasound for 40–60 min. The antioxidant activity of HBG treated by ultrasound with different time was increased first and then decreased. Among the studied ultrasound time, 30 min proved to be an effective time range with excellent antioxidant properties. The enhanced antioxidant activity may be due to smaller molecules taking less time to reach the target substance and scavenge or terminate the chain reaction. Furthermore, the results of Congo red and FT-IR spectrum indicated that ultrasound irradiation caused the stretching of polymeric chains and breaking β-glyosidic linkage of HBG without altering its primary functional groups. In addition, the change of HBG micromorphology was time-dependent. When the ultrasonic time is $<$30 min, ultrasonic cavitation depolymerized large sphere aggregates of native HBG into small round fragments by untwisting the HBG chains. The depolymerization was probably attributed to the chain disentanglement resulting from the reduction of intra- and intermolecular hydrogen bonds However, the stretched HBG molecular chains were further reaggregated with the extension of ultrasonic time. In summary, the highest free radicals scavenging activity in HBG resulted from its smallest molecular size, which revealed that ultrasound has potential value in improving the antioxidant activity of HBG through structural changes.

Author statement

I have made substantial contributions to the conception or design of the work; or the acquisition analysis, or interpretation of data for work; I have drafted the work or revised it critically for important intellectual content; I have approved the final version to be published; I agree to be the accountable for all aspects of the work in ensuring that questions related to the accuracy or integrity of any part of the work are appropriately investigated and resolved.

CRediT authorship contribution statement

Hongwei Cao: Investigation, Conceptualization, Writing - original draft. **Xiaoxue Wang:** Writing - review & editing. **Mengmeng Shi:** Data curation, Software. **Xiao Guan:** Funding acquisition, Supervision. **Chunhong Zhang:** Data curation. **Yueqin Wang:** Visualization. **Linnan Qiao:** Methodology. **Hongdong Song:** Visualization. **Yu Zhang:** Data curation.

Declaration of Competing Interest

The authors declare that they have no known competing financial interests or personal relationships that could have appeared to influence the work reported in this paper.

Data availability

No data was used for the research described in the article.

Acknowledgments

This work was supported by the Domestic Science and Technology Cooperation Projects of Shanghai (21015801100), Shanghai Sailing Program (20YF1433400); National Natural Science Foundation of China (32102140); Young Elite Scientists Sponsorship Program by CAST (2021QNRC001).

Appendix A. Supplementary data

Supplementary data to this article can be found online at https://doi.org/10.1016/j.fochx.2023.100793.

References

Al-Ansi, et al. (2021). Characterization of molecular, physicochemical, and morphological properties of starch isolated from germinated highland barley, 101052 *Food Bioscience, 42*. https://doi.org/10.1016/j.fbio.2021.101052.

Alzorqi, et al. (2016). Optimization of ultrasound induced emulsification on the formulation of palm-olein based nanoemulsions for the incorporation of antioxidant β-d-glucan polysaccharides. *Ultrasonics Sonochemistry, 31*, 71–84. https://doi.org/10.1016/j.ultsonch.2015.12.004

Bai, et al. (2021). Effect of thermal processing on the molecular, structural, and antioxidant characteristics of highland barley β-glucan, 118416 *Carbohydrate Polymers, 271*. https://doi.org/10.1016/j.carbpol.2021.118416.

Błaszczyk, et al. (2015). Impact of low and high molecular weight oat beta-glucan on oxidative stress and antioxidant defense in spleen of rats with LPS induced enteritis. *Food Hydrocolloids, 51*, 272–280. https://doi.org/10.1016/j.foodhyd.2015.05.025

Cai, et al. (2018). Effect of ultrasound on size, morphology, stability and antioxidant activity of selenium nanoparticles dispersed by a hyperbranched polysaccharide from Lignosus rhinocerotis. *Ultrasonics Sonochemistry, 42*, 823–831. https://doi.org/10.1016/j.ultsonch.2017.12.022

Cai, et al. (2022). Ultrasound-induced changes in rheological behavior and hydrophobic microdomains of Lignosus rhinocerotis polysaccharide. *International Journal of Biological Macromolecules, 213*, 565–573. https://doi.org/10.1016/j.ijbiomac.2022.05.182

Chen, et al. (2014). Structure and properties of a (1→3)-β-d-glucan from ultrasound-degraded exopolysaccharides of a medicinal fungus. *Carbohydrate Polymers, 106*, 270–275. https://doi.org/10.1016/j.carbpol.2014.02.040

Chen, et al. (2021a). Free radical-mediated degradation of polysaccharides: Mechanism of free radical formation and degradation, influence factors and product properties, 130524 *Food Chemistry, 365*. https://doi.org/10.1016/j.foodchem.2021.130524.

Chen, et al. (2021b). Physicochemical and functional characteristics of polysaccharides from okra extracted by using ultrasound at different frequencies, 130138 *Food Chemistry, 361*. https://doi.org/10.1016/j.foodchem.2021.130138.

Cui, & Zhu. (2021). Ultrasound modified polysaccharides: A review of structure, physicochemical properties, biological activities and food applications. *Trends in Food Science & Technology, 107*, 491–508. https://doi.org/10.1016/j.tifs.2020.11.018

Du, et al. (2022). Critical review on alterations in physiochemical properties and molecular structure of natural polysaccharides upon ultrasonication, 106170 *Ultrasonics Sonochemistry, 90*. https://doi.org/10.1016/j.ultsonch.2022.106170.

Faure, & Nyström. (2016). Effect of apotransferrin, lactoferrin and ovotransferrin on the hydroxyl radical mediated degradation of beta-glucan. *Food Chemistry, 204*, 1–6. https://doi.org/10.1016/j.foodchem.2016.02.075

Feng, et al. (2021). Effects of multi-mode divergent ultrasound pretreatment on the physicochemical and functional properties of polysaccharides from Sagittaria sagittifolia L. *Food Bioscience, 42*, Article 101145. https://doi.org/10.1016/j.fbio.2021.101145

Gao, et al. (2022). Optimization of ultrasonic-assisted polysaccharide extraction from Hyperici Perforati Herba using response surface methodology and assessment of its antioxidant activity. *International Journal of Biological Macromolecules*. https://doi.org/10.1016/j.ijbiomac.2022.10.260

Giese, et al. (2015). Free-radical scavenging properties and antioxidant activities of botryosphaeran and some other β-D-glucans. *International Journal of Biological Macromolecules, 72*, 125–130. https://doi.org/10.1016/j.ijbiomac.2014.07.046

Gokce, et al. (2014). Ultrasonication of chitosan nanoparticle suspension: Influence on particle size. *Colloids and Surfaces A: Physicochemical and Engineering Aspects, 462*, 75–81. https://doi.org/10.1016/j.colsurfa.2014.08.028

Guo, et al. (2020). Understanding the nutrient composition and nutritional functions of highland barley (Qingke): A review. *Trends in Food Science & Technology, 103*, 109–117. https://doi.org/10.1016/j.tifs.2020.07.011

Hong, et al. (2023). Effects of different thermal processing methods on bioactive components, phenolic compounds, and antioxidant activities of Qingke (highland hull-less barley). *Food Science and Human Wellness, 12*(1), 119–129. https://doi.org/10.1016/j.fshw.2022.07.030

Hu, et al. (2021). Structure, size and aggregated morphology of a β-D-glucan from Lignosus rhinocerotis as affected by ultrasound, 118344 *Carbohydrate Polymers, 269*. https://doi.org/10.1016/j.carbpol.2021.118344.

Huang, et al. (2022). Intervention of microwave irradiation on structure and quality characteristics of quinoa protein aggregates, 107677 *Food Hydrocolloids, 130*. https://doi.org/10.1016/j.foodhyd.2022.107677.

Khan, et al. (2016). Structural, thermal, functional, antioxidant & antimicrobial properties of β-d-glucan extracted from baker's yeast (Saccharomyces cereviseae)—Effect of γ-irradiation. *Carbohydrate Polymers, 140*, 442–450. https://doi.org/10.1016/j.carbpol.2016.01.003

Li, et al. (2022a). Highland barley improves lipid metabolism, liver injury, antioxidant capacities and liver functions in high-fat/cholesterol diet mice based on gut microbiota and LC-MS metabonomics, 102094 *Food Bioscience, 50*. https://doi.org/10.1016/j.fbio.2022.102094.

Li, et al. (2017). Morphology and Structural Properties of Novel Short Linear Glucan/Protein Hybrid Nanoparticles and Their Influence on the Rheological Properties of Starch Gel. *Journal of Agricultural and Food Chemistry, 65*(36), 7955–7965. https://doi.org/10.1021/acs.jafc.7b02800

Li, et al. (2022b). Preparation and characterization of feruloylated oat β-glucan with antioxidant activity and colon-targeted delivery, 119002 *Carbohydrate Polymers, 279*. https://doi.org/10.1016/j.carbpol.2021.119002.

Li, et al. (2023). Structure characteristics of low molecular weight pectic polysaccharide and its anti-aging capability by modulating the intestinal homeostasis, 120467 *Carbohydrate Polymers, 303*. https://doi.org/10.1016/j.carbpol.2022.120467.

Li, et al. (2021). Comparison of distribution and physicochemical properties of β-glucan extracted from different fractions of highland barley grains. *International Journal of Biological Macromolecules, 189*, 91–99. https://doi.org/10.1016/j.ijbiomac.2021.08.094

Liu, et al. (2021). Comparison of physicochemical properties of β-glucans extracted from hull-less barley bran by different methods. *International Journal of Biological Macromolecules, 182*, 1192–1199. https://doi.org/10.1016/j.ijbiomac.2021.05.043

Luo, et al. (2023). Simultaneously enhanced stability and biological activities of chlorogenic acid by covalent grafting with soluble oat β-glucan, 100546 *Food Chemistry: X, 17*. https://doi.org/10.1016/j.fochx.2022.100546.

Ma, et al. (2022). Effects of ultrasound-assisted H2O2 on the solubilization and antioxidant activity of yeast β-glucan, 106210 *Ultrasonics Sonochemistry, 90*. https://doi.org/10.1016/j.ultsonch.2022.106210.

Mosele, et al. (2018). Beta-Glucan and Phenolic Compounds: Their Concentration and Behavior during in Vitro Gastrointestinal Digestion and Colonic Fermentation of Different Barley-Based Food Products. *Journal of Agricultural and Food Chemistry, 66*(34), 8966–8975. https://doi.org/10.1021/acs.jafc.8b02240

Obadi, et al. (2021). Highland barley: Chemical composition, bioactive compounds, health effects, and applications, 110065 *Food Research International, 140*. https://doi.org/10.1016/j.foodres.2020.110065.

Tang, et al. (2021). Impact of germination pretreatment on the polyphenol profile, antioxidant activities, and physicochemical properties of three color cultivars of highland barley, 103152 *Journal of Cereal Science, 97*. https://doi.org/10.1016/j.jcs.2020.103152.

Wang, et al. (2021). Ultrasound irradiation alters the spatial structure and improves the antioxidant activity of the yellow tea polysaccharide, 105355 *Ultrasonics Sonochemistry, 70*. https://doi.org/10.1016/j.ultsonch.2020.105355.

Wang, et al. (2017). Ultrasonic Method to Synthesize Glucan-g-poly(acrylic acid)/Sodium Lignosulfonate Hydrogels and Studies of Their Adsorption of Cu2+ from Aqueous Solution. *ACS Sustainable Chemistry & Engineering, 5*(8), 6438–6446. https://doi.org/10.1021/acssuschemeng.7b00332

Xi, et al. (2023). The structural and functional properties of dietary fibre extracts obtained from highland barley bran through different steam explosion-assisted treatments, 135025 *Food Chemistry, 406*. https://doi.org/10.1016/j.foodchem.2022.135025.

Xia, et al. (2018). Antioxidant activity of whole grain Qingke (Tibetan Hordeum vulgare L.) toward oxidative stress in d-galactose induced mouse model. *Journal of Functional Foods, 45*, 355–362. https://doi.org/10.1016/j.jff.2018.04.036

Xie, et al. (2022). In Vitro and In Vivo Digestive Fate and Antioxidant Activities of Polyphenols from Hulless Barley: Impact of Various Thermal Processing Methods and β-Glucan. *Journal of Agricultural and Food Chemistry, 70*(25), 7683–7694. https://doi.org/10.1021/acs.jafc.2c01784

Xiong, et al. (2022). The difference among structure, physicochemical and functional properties of dietary fiber extracted from triticale and hull-less barley, 112771 *LWT, 154*. https://doi.org/10.1016/j.lwt.2021.112771.

Xu, et al. (2022). Effects of ultrasound-assisted Fenton treatment on structure and hypolipidemic activity of apricot polysaccharides, 102073 *Food Bioscience, 50*. https://doi.org/10.1016/j.fbio.2022.102073.

Yan, et al. (2021). Preparation and characterization of curdlan with unique single-helical conformation and its assembly with Congo Red, 117985 *Carbohydrate Polymers, 263*. https://doi.org/10.1016/j.carbpol.2021.117985.

Yang, & Huang. (2021). Extraction methods and activities of natural glucans. *Trends in Food Science & Technology, 112*, 50–57. https://doi.org/10.1016/j.tifs.2021.03.025
Ye, et al. (2021). Structure and physicochemical properties of arabinan-rich acidic polysaccharide from the by-product of peanut oil processing, 106743 *Food Hydrocolloids, 117*. https://doi.org/10.1016/j.foodhyd.2021.106743.
Yuan, et al. (2020). Ultrasonic degradation effects on the physicochemical, rheological and antioxidant properties of polysaccharide from Sargassum pallidum, 116230 *Carbohydrate Polymers, 239*. https://doi.org/10.1016/j.carbpol.2020.116230.
Zang, et al. (2023). Effects of highland barley β-glucan on blood glucose and gut microbiota in streptozotocin-induced, diabetic, C57BL/6 mice on a high-fat diet, 111882 *Nutrition, 107*. https://doi.org/10.1016/j.nut.2022.111882.
Zhang, et al. (2021). Fractionation, chemical characterization and immunostimulatory activity of β-glucan and galactoglucan from Russula vinosa Lindblad, 117559 *Carbohydrate Polymers, 256*. https://doi.org/10.1016/j.carbpol.2020.117559.
Zhao, et al. (2013). Ultrasound extraction optimization of Acanthopanax senticosus polysaccharides and its antioxidant activity. *International Journal of Biological Macromolecules, 59*, 290–294. https://doi.org/10.1016/j.ijbiomac.2013.04.067
Zhao, et al. (2020). Different aggregation states of barley β-glucan molecules affects their solution behavior: A comparative analysis, 105543 *Food Hydrocolloids, 101*. https://doi.org/10.1016/j.foodhyd.2019.105543.
Zheng, et al. (2021). Different molecular sizes and chain conformations of water-soluble yeast β-glucan fractions and their interactions with receptor Dectin-1, 118568 *Carbohydrate Polymers, 273*. https://doi.org/10.1016/j.carbpol.2021.118568.
Zhou, et al. (2022). Protective effects of black onion polysaccharide on liver and kidney injury in T2DM rats through the synergistic impact of hypolipidemic and antioxidant abilities. *International Journal of Biological Macromolecules, 223*, 378–390. https://doi.org/10.1016/j.ijbiomac.2022.11.055